Photophysical Properties of PS-2 Reaction Centers and a Discrepancy in Exciton Relaxation Times†

Thomas Renger and R. A. Marcus*

Noyes Laboratory of Chemical Physics, Mail Code 127-72, Pasadena, California 91125

Received: August 29, 2001; In Final Form: November 29, 2001

Exciton relaxation in the PS-2 reaction center of green plants is studied to explain a discrepancy of 2 orders of magnitude in certain relaxation times. Structural information from an earlier computer model and a recent low resolution structural study are combined with circular dichroism (CD) at 77 K, fluorescence line narrowing spectra at 1.6 K, and pump−probe spectra at 77 K to make predictions on the linear absorption spectrum at 77 K, fluorescence spectrum at 5 K, and absorption difference spectrum for modified pheophytin of the D_2 branch at 5 K. A width of the inhomogeneous distribution function of pigment energies of $\Delta_{inh} = 300$ cm^{-1} and a mean vertical pigment transition energy corresponding to 669 nm are assumed for all pigments, based on the CD data, and a correlation radius of 5 Å for the protein vibrations is deduced from the pump−probe data. The two peripheral chlorophylls resolved in a recent structure are calculated to give rise to optical dephasing times larger than 10 ps at wavelengths shorter than 670 nm, in agreement with dephasing times obtained in hole burning experiments. It is proposed, thereby, that the 2 orders of magnitude discrepancy between the fastest transfer times observed in hole burning and these in pump−probe experiments is due to the peripheral chlorophylls. Non-Markovian effects in the exciton-vibrational coupling are found to contribute significantly to optical line shape functions in the form of vibrational sidebands but to have minor influence on the relaxation dynamics of the excitons.

I. Introduction

The microscopic structure of the PS-2 reaction center of green plants was determined by electron cryomicroscopy of two-dimensional crystals at a resolution of 8 Å.[1] Very recently a 3.8 Å resolution X-ray structural study by Zouni et al.[2] was also published. These studies reveal a structure strikingly similar to that of the bacterial reaction center, for which a high resolution (2.8 Å) study has existed for more than a decade.[3] From these similarities it was inferred that both reaction centers have a common evolutionary origin,[1] as predicted earlier.[4]

A major difference between the two reaction centers is that the distance of 10.0 Å within the so-called special pair in the PS-2 reaction center[2] is larger than the 7.6 Å distance in the bacterial reaction center.[4] This difference, which had been predicted earlier,[5−9] has dramatic effects on the observed optical spectra. The optical transitions of the different pigments in the bacterial reaction center are well separated in energy, but the overall PS-2 absorption band is much narrower. In particular, it contains almost no structure, because of strongly overlapping optical lines and inhomogeneous broadening (e.g., ref 10). Although this aspect largely complicates theoretical studies, it is also a challenge to understand the advantage, if any, of this particular change in the distance between two pigments that occurred in natural evolution. Because of the larger distance within the special pair of the PS-2 reaction center, all six core pigments are more or less equal, in terms of intermolecular interactions and closest distances to neighboring pigments. The low-energy exciton states therefore are not as red-shifted from the exciton states of the surrounding antennae as in the bacterial reaction center. This circumstance makes the PS-2 reaction center a shallower trap for excitation energy.

† As presented at the conference *Biophysical Aspects of Electron and Proton Transfer*, Hünfeld, May 24−27, 2001.

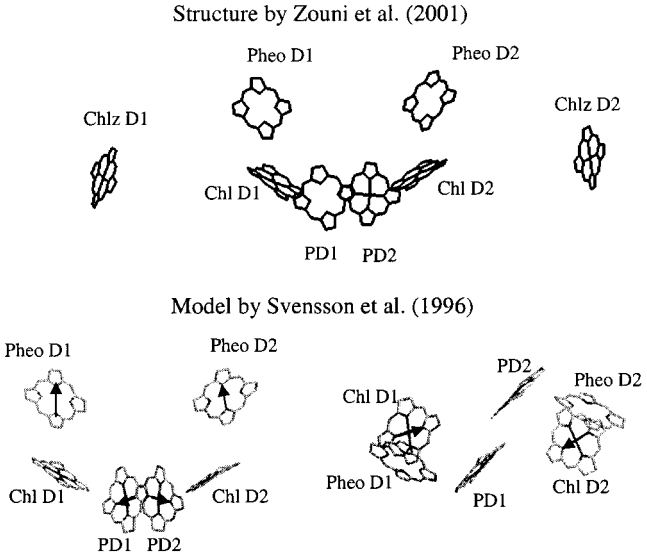

Figure 1. Arrangement of core pigments in the recent 3.8 Å structural study[2] (top) compared to an earlier computer model by Svensson et al.[8] (bottom). The optical transition dipole geometries suggested in the latter for the six core pigments are shown.

An atomic model for the PS-2 reaction center core has been developed,[8,9] using methods from computational chemistry. The correct distance within the special pair and the correct overall structure for the protein was predicted from the computational model,[8,9] which was based on the known structure of the bacterial reaction center as an input for the structure optimization routine. The atomic model of the six core pigments in the computational model[8] is compared with the recent 3.8 Å structure[2] in Figures 1 and 2. The interpigment center-to-center distances of the six core pigments, which consist of the special

10.1021/jp013342f CCC: $22.00
Published on Web 01/30/2002

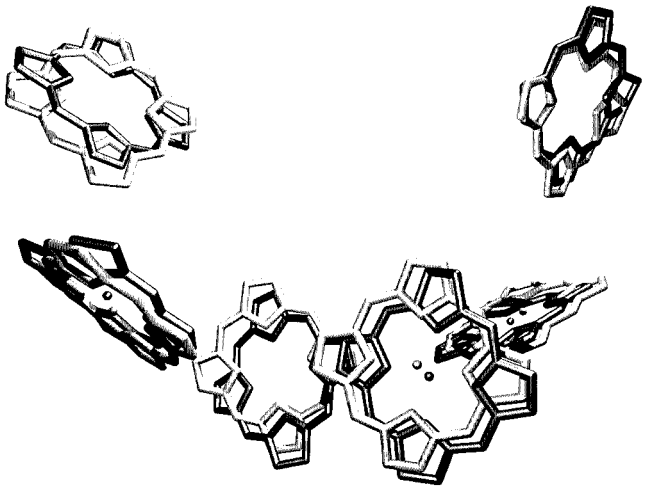

Figure 2. Overlay of the porphyrin skeletons of the six core pigments from the recent X-ray structure[2] (drawn in gray) and an earlier computer model[8] (drawn in black).

pair P_{D1}, P_{D2}, the two accessory chlorophylls Chl_{D1}, Chl_{D2}, and the two pheophytins $Pheo_{D1}$, $Pheo_{D2}$, agree within ± 1 Å. For example, the distance in the special pair between P_{D1} and P_{D2} is 10.3 Å in Svensson's model,[8] compared with 10.0 Å form Zouni's 3.8 Å structural study.[2] There are, however, two differences between the two studies that are important for the model that is presented here.

The first difference concerns the two peripheral chlorophylls $Chlz_{D1}$ and $Chlz_{D2}$ that were absent in the computer model by Svensson et al.[8] but appear in the structural study of ref 2. These two pigments interact only weakly with the core pigments. Their position at the periphery of the reaction center core brings them near the CP43 and CP47 core antenna complexes which surround the D1-D2 protein.[1,2,11] The two peripheral chlorophyll pigments can provide thereby a pathway for the transfer of excitation energy from the antennae to the reaction center. Alternatively, the excitation energy may also be transferred directly from CP43 and CP47 to the six core pigments, as suggested by the intermolecular distances in the recent structural study.[2] The peripheral chlorophyll situated on the D_1 site of the reaction center can also serve as an intermediate in the electron-transfer reaction between cytochrome b_{559} and the oxidized special pair $P680^+$.[12]

A second difference between the computer model[8] and the X-ray structural study is that the 3.8 Å resolution obtained in the latter did not allow a resolution of the optical transition dipole geometry of the pigments. The computer model of ref 8 yielded the orientation for the optical transition dipole moments shown in Figure 1. We use the close resemblance of the orientations of porphyrin skeletons of the pigments in the two studies, based on the model of Svensson et al.,[8] to assign the dipole moments in the structural study of Zouni et al.[2] An overlay of the porphyrin skeletons assigned in the two studies is shown in Figure 2.

There are a number of interesting experimental results to be explained in the optical experiments on the PS-2 reaction center. A recent review of this topic was given in ref 13. There is the usual question of why, in a reaction center core arranged in approximate 2-fold symmetry, electron transfer proceeds exclusively along one branch.[14,15] The identity of the primary electron donor has also become a matter of discussion.[10,16] In addition there is the question about the relative time scales of energy and charge-transfer[17] reactions in the PS-2 reaction center.

The present study was prompted by the deviations in experimentally determined energy transfer (exciton relaxation) times: From hole burning studies time constants of 50 and 12 ps were estimated for energy transfer from the pheophytin and the accessory chlorophyll to the special pair.[20] These hole burning values contrast with pump−probe experiments, which give the fastest equilibration times among the excited states as being on a subpicosecond time scale,[21−23] in addition to picosecond components.[22,24−27] Several possible sources for a multiexponential decay of excitons are examined in the present article for the various phenomena: (i) disorder in energies and intermolecular couplings, (ii) memory effects in the exciton vibrational coupling, and (iii) heterogeneity in site energies and couplings.

We employ the multimer model[28] for the PS-2 reaction center, in which the site energies and inhomogeneous widths are assumed equal for all pigments. Its dissipative exciton dynamics has been studied[29] and used to calculate the transient absorption spectra measured in the red wing of the absorption spectrum. For that wing the small excited-state absorption can be neglected. The same multimer model has been used for the calculation of two-pulse photon echo spectra.[16]

These studies are extended in the present paper by including two-exciton states (e.g., refs 30 and 31) and incorporating optical transitions between the one-and the two-exciton manifolds into the theory. The extension permits the study of the dependence of the shift of the entire nonlinear absorption spectrum on the delay time between the pump and probe pulses. Because of the recent structural study it is now possible to include also the two peripheral chlorophylls.

Another aspect of the theory concerns the inclusion of dynamic disorder, in particular the modulation of pigment transition energies and couplings by the protein dynamics. The exciton-vibrational coupling is described in standard density matrix theories by a spectral density $J(\omega)$, (e.g., refs 31 and 32). A frequency-independent spectral density was used in ref 28. A more realistic spectral density was estimated[16] from fluorescence line narrowing spectra[33] of PS-2 reaction centers. The spectral density for the local pigment−protein coupling in the present paper was evaluated[34] from fluorescence line narrowing spectra[35] of the B777-complex, a single-pigment protein complex. The exciton-vibrational coupling is then described below within a non-Markovian theory. The latter also provides information on the validity of the Markov approximation applied earlier.[16,29]

When non-Markovian effects are studied different summation techniques[36−39] for the exciton-vibrational coupling can be used, as discussed in detail elsewhere.[34] The so-called POP (partial ordering prescription) equation allows one to include the diagonal parts of the exciton-vibrational coupling exactly, whereas the alternative COP[40] (chronological ordering prescription) contains only a partial summation of this coupling. This difference was demonstrated[34] to result in COP failing to describe the vibrational sidebands in fluorescence line-narrowing spectra of B820 complexes, whereas POP gave agreement with this experiment. Such an experiment is designed to resolve the homogeneous line-shape function of optical transitions. As demonstrated earlier[34] for inhomogeneous spectra, both treatments, POP and COP, result in very similar plots due to the disorder involved in the averaging.

In an earlier study[41] of the absorption of PS-2 reaction centers, the standard spin-boson type theory[42−44] was applied to include the vibrational sidebands of the optical transitions of the pigments. However, the coupling between the pigments was

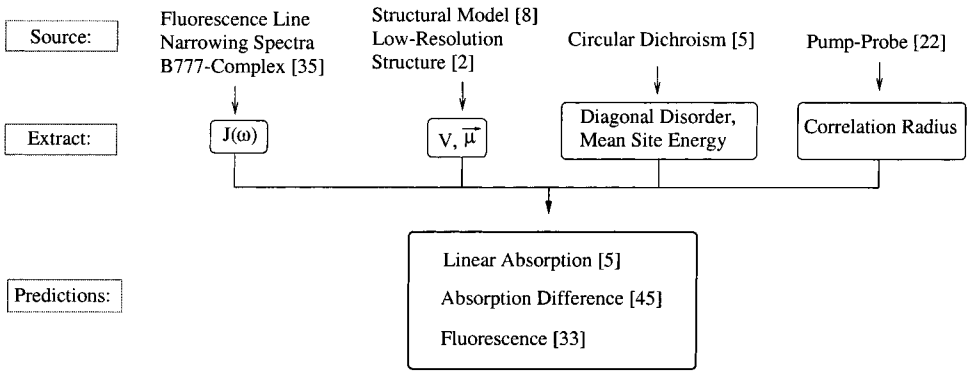

Figure 3. Input data, extraction of parameters and predictions.

neglected there, because there was no theory that was able to treat both the interpigment coupling and the pigment−protein coupling on the same footing. Such a theory was developed recently[34] and is applied here.

The paper is organized as follows. In section II the linear optical properties of PS-2 reaction centers are studied. The 77 K circular dichroism spectrum[5] is used to estimate two of the three parameters of the model, the third parameter being determined from the calculation of 77 K pump−probe spectra. The model is then used to simulate the 77 K linear absorption spectrum,[5] the 5 K fluorescence spectrum,[33] and a 5 K absorption difference spectrum,[45] in which the pheophytin of the D2 branch $Pheo_{D2}$ was chemically replaced by a deoxo-hydroxy pheophytin. In section III it is examined how the two peripheral pigments contribute to optical dephasing times at different wavelengths. In addition, the nonlinear optical response is calculated and compared with measured 77 K pump−probe spectra.[22] In section IV these various results are discussed, and an explanation of the factor of 100 discrepancy in lifetimes is given in the role of the two peripheral chlorophylls. The paper is summarized in section V. We describe in Figure 3 the input data of the theory, the quantities extracted, and the predictive consequences for three different experiments.

II. Calculation of Circular Dichroism, Linear Absorption, Linear Absorption Difference, and Fluorescence Spectra

A simplified model, the point-dipole approximation, is used to treat the interaction between the locally excited states of the aggregate in the present paper. The methods used here can be extended to include more general interactions,[46−49] but we believe the present approach provides a useful starting point.

The interaction is expressed as a dipole−dipole coupling between the optical transition dipoles. Since the recent 3.8 Å X-ray study[2] did not resolve the geometry of the transition dipoles of the pigments, an alternative strategy was chosen. To decide for each pigment whether the transition dipole is parallel to its N_A-N_C axis or to its N_B-N_D axis (N_A to N_D as defined in the Brookhaven Data Bank File 1FE1[60a]) it was first established which of the two orientations more closely resembles the dipole orientation given in Svensson's computer model.[8] On this basis the orientations for the pigments (P_{D1}, P_{D2}, Chl_{D1}, Chl_{D2}, $Pheo_{D1}$, $Pheo_{D2}$, $Chlz_{D1}$, $Chlz_{D2}$) were assigned as (1, 0, 1, −1, −0, 1, 1, 0), where zero and one represent dipoles along the N_A-N_C axis and N_B-N_D axis, respectively, as assigned in the file 1FE1.pdb, and −1 and −0 are dipoles in the N_D-N_B and N_C-N_A directions, respectively.[60b] Since for chlorophylls and pheophytins the Q_y transition diploe moment is generally assumed to be oriented along the N_B-N_D (N_I-N_{III}) axis, the assignment of N_A-N_C given in the file 1FE1.pdb has to be interchanged with N_B-N_D for P_{D2} and with N_D-N_B for $Pheo_{D1}$ on the basis of the present comparison with the Svennson model. The dipole orientations for the two peripheral pigments $Chlz_{D1}$ and $Chlz_{D2}$ were chosen arbitrarily, these pigments being absent in the Svensson model.[8] However, the present results do not depend critically on this assignment, since similarly small couplings of the peripheral chlorophylls to the six core pigments are obtained for the other possible orientations. The dipole−dipole couplings calculated in this way are given in Table 1. Using these couplings and a given set of site energies for the pigments, the one-exciton states are obtained from a diagonalization, yielding energies ϵ_M, optical transition dipole moments $\vec{\mu}_M$, and rotational strengths r_M of the one-exciton states $|M\rangle$.

TABLE 1: Calculated Dipole−Dipole Interactions in PS-2 Reaction Centers in Units of cm^{-1} [a]

	P_{D2}	Chl_{D1}	Chl_{D2}	$Pheo_{D1}$	$Pheo_{D2}$	$Chlz_{D1}$	$Chlz_{D2}$
P_{D1}	139	−54	−84	−15	18	1	−1
P_{D2}		−85	−56	19	−13	−1	5
Chl_{D1}			9	87	−5	−6	2
Chl_{D2}				−6	92	0	−3
$Pheo_{D1}$					5	4	−1
$Pheo_{D2}$						0	0
$Chlz_{D1}$							0

[a] The atomic coordinates of the pigments of the D_1 and D_2 branches of the PS-2 reaction center were obtained from the Brookhaven Protein Data Bank (file 1FE1.pdb). The following dipole-strengths have been assumed,[8] $d_{S_0\rightarrow S_1} = 4.8$ D for the Chls and $d_{S_0\rightarrow S_1} = 3.72$ D for the Pheos.

The following equations are based on the POP equation of motion for the density matrix and include a Markov approximation for the off-diagonal parts of the exciton-vibrational coupling. An alternative COP formalism and the resulting optical spectra are given in Appendix C. The Markov approximation for the off-diagonal parts will be investigated later in the calculation of pump−probe spectra.

The spectra for circular dichroism CD(ω) and linear absorption $\alpha(\omega)$ can then be written as[34]

$$\mathrm{CD}(\omega) \propto \langle \sum_M r_M D_M(\omega) \rangle_{\mathrm{dis}} \tag{1}$$

$$\alpha(\omega) \propto \langle \sum_M |\mu_M|^2 D_M(\omega) \rangle_{\mathrm{dis}} \tag{2}$$

where $\langle\ \rangle_{\mathrm{dis}}$ is an average over static disorder in site energies. A Gaussian distribution function of width (fwhm) Δ_{dis} is assumed for these energies, and the disorder average is performed numerically. The line shape function $D_M(\omega)$ reads[34]

$$D_M(\omega) = Re \int_0^\infty \mathrm{d}t\, \mathrm{e}^{i(\omega-\tilde{\omega}_{M0})t}\, \mathrm{e}^{G_M(t)-G_M(0)}\, \mathrm{e}^{-t/\tau_M} \tag{3}$$

where $\tilde{\omega}_{M0}$ is the transition frequency between the minima of the ground-state potential energy surface (PES) and the PES of the Mth exciton state (the $0 \rightarrow 0$ transition)

$$\tilde{\omega}_{M0} = \omega_{M0} - \gamma_{MM}E_\lambda/\hbar + \sum_K (1 - \delta_{MK})\gamma_{MK}\tilde{C}^{(\mathrm{Im})}(\omega_{MK}) \quad (4)$$

with $\omega_{M0} = \epsilon_M/\hbar$ being the vertical transition energy at the minimum position of the ground-state PES, E_λ is the reorganization energy[32]

$$E_\lambda/\hbar = \int_0^\infty \mathrm{d}\omega\, \omega J(\omega) \quad (5)$$

and γ_{MK} is an exciton-vibrational coupling constant that depends on the eigencoefficients $c_m^{(M)}$ of exciton states and on the correlation radius of protein vibrations R_c,

$$\gamma_{MK} = \sum_{m,n} \mathrm{e}^{-R_{mn}/R_c} c_m^{(M)} c_m^{(K)} c_n^{(M)} c_n^{(K)} \quad (6)$$

and $\tilde{C}^{(\mathrm{Im})}(\omega_{MK})$ is the imaginary part of $\tilde{C}(\omega)$:[31,34,40]

$$\tilde{C}(\omega) = \pi\omega^2\{(1 + n(\omega))J(\omega) + n(-\omega)J(-\omega)\} + i\frac{1}{\pi}\mathcal{P}\int_{-\infty}^{\infty} \mathrm{d}\bar{\omega}\, \frac{\tilde{C}^{(Re)}(\bar{\omega})}{\omega - \bar{\omega}} \quad (7)$$

where $\omega = \omega_{MK}$ and $\tilde{C}^{(Re)}(\bar{\omega})$ is the first part in the rhs of eq 7 with $\omega = \bar{\omega}$. The time-dependent function $G_M(t)$ in eq 3 is[34]

$$G_M(t) = \gamma_{MM}\int_{-\infty}^{\infty} \mathrm{d}\omega\, \mathrm{e}^{-i\omega t}\{(1 + n(\omega))J(\omega) + n(-\omega)J(-\omega)\} \quad (8)$$

and the reciprocal of the dephasing time in eq 3 is[31,34]

$$\tau_M^{-1} = \sum_K \gamma_{MK}\tilde{C}^{(Re)}(\omega_{MK}) \quad (9)$$

The temperature dependence of the optical line shape function $D_M(\omega)$ is given by the Bose−Einstein distribution function $n(\omega) = (\mathrm{e}^{\hbar\omega/kT} - 1)^{-1}$ entering eq 3 via eqs 7 and 8. The spectral density $J(\omega)$ in eqs 7 and 8 was extracted[34] from the 1.6 K fluorescence line narrowing spectra measured[35] for B777 complexes as

$$J(\omega) = \sum_{i=1,2} \frac{s_i}{7!2\omega_i^4}\omega^3\, \mathrm{e}^{-(\omega/\omega_i)^{1/2}} \quad (10)$$

The numerical coefficient in eq 10 was chosen so that $\int_0^\infty \mathrm{d}\omega J(\omega)$ equals the Huang−Rhys factor, $s_1 + s_2$. The extracted parameters are $s_1 = 0.8$, $s_2 = 0.5$, $\hbar\omega_1 = 0.069$ meV, and $\hbar\omega_2 = 0.24$ meV. The scheme of the equations used to extract the spectral density is given in Appendix A.

The fluorescence signal is obtained as[34]

$$I(\omega) \propto \sum_M \left\langle \frac{\mathrm{e}^{-\hbar\omega_{M0}/kT}}{\sum_N \mathrm{e}^{-\hbar\omega_{N0}/kT}} \left|\mu_M\right|^2 D'_M(\omega) \right\rangle_{\mathrm{dis}} \quad (11)$$

with the line shape function $D'_M(\omega)$ being[34]

$$D'_M(\omega) = Re\int_0^\infty \mathrm{d}t\, \mathrm{e}^{i(\omega - \tilde{\omega}'_{M0})t}\, \mathrm{e}^{(G_M(t))^* - G_M(0)}\, \mathrm{e}^{-t/\tau'_M} \quad (12)$$

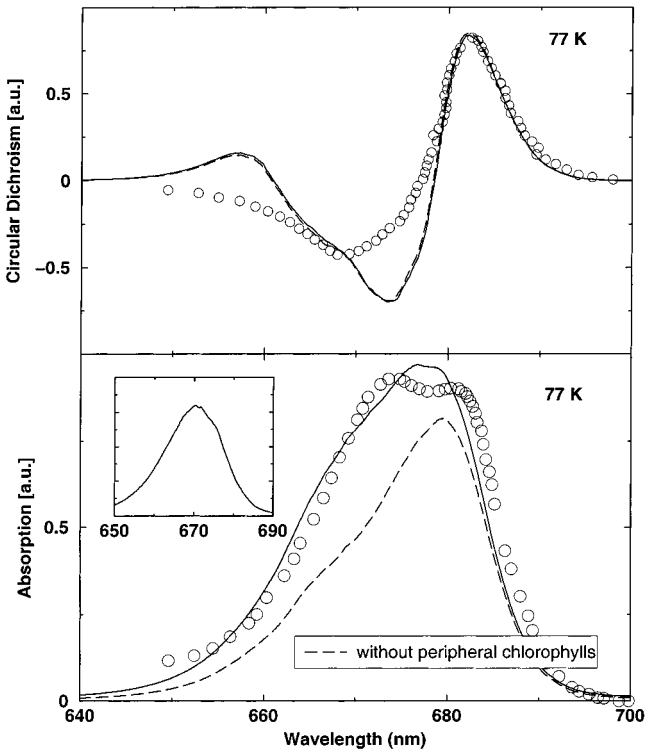

Figure 4. Calculation of 77 K circular dichroism spectrum (shown in the top part) and linear absorption (bottom part) spectrum using a POP treatment. The solid lines were obtained including all pigments in the calculation, for the dashed lines the two peripheral pigments were omitted. Circles show the experimental data measured by Tetenkin et al.[5] The absorption difference spectrum (solid minus dashed line) is shown as an inset in the lower part.

where

$$\tilde{\omega}'_{M0} = \omega_{M0} - \gamma_{MM}E_\lambda/\hbar + \sum_K (1 - \delta_{MK})\gamma_{MK}\tilde{C}^{(\mathrm{Im})}(\omega'_{MK}) \quad (13)$$

and

$$1/\tau'_M = \sum_K \gamma_{MK}\tilde{C}^{(Re)}(\omega'_{MK}) \quad (14)$$

with $\omega'_{MK} = \omega'_{M0} - \omega'_{K0}$, where the transition frequencies ω'_{K0} are

$$\omega'_{K0} = \omega_{K0} - 2\gamma_{MK}E_\lambda/\hbar \quad (15)$$

Various linear optical properties of PS-2 reaction centers are calculated next, using the above equations. The circular dichroism spectrum yields 14948 cm^{-1} (669 nm) for a mean vertical transition energy of the pigments and $\Delta_{\mathrm{dis}} = 300$ cm^{-1} for a local inhomogeneous width. For the correlation radius R_c a value of 5 Å was used, determined later from the pump−probe spectra. However, the presented linear optical spectra do not depend critically on this value. The CD spectrum calculated is compared with the experimental data of Tetenkin et al.[5] in the upper half of Figure 4.

In the lower half of this figure the linear absorption spectrum measured by Tetenkin et al.[5] is compared with the theoretical prediction resulting from the above three parameters. The dashed lines are obtained when the two peripheral pigments are omitted in the calculation. As seen in the upper half of Figure 4 these pigments barely influence the CD spectrum. This result is expected, since the CD vanishes when interpigment couplings are absent. In contrast, the peripheral chlorophylls are a major

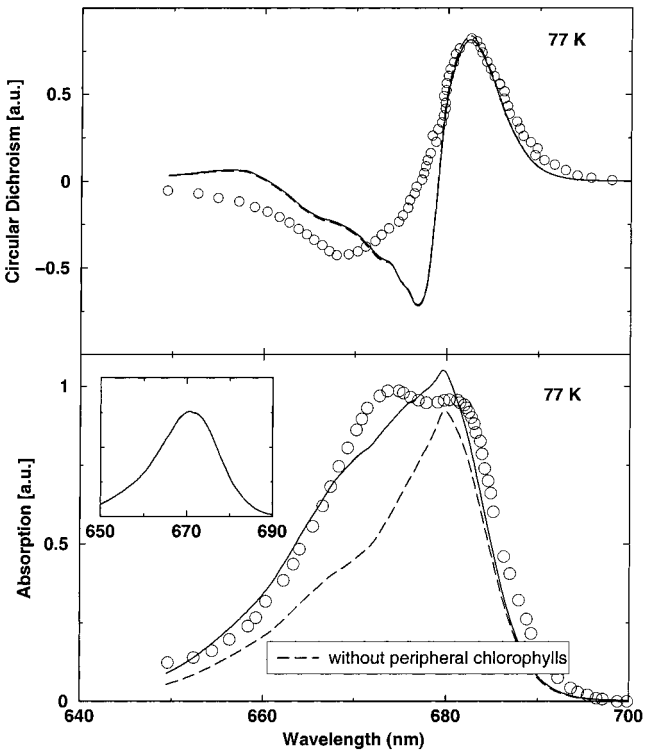

Figure 5. Same as in Figure 4 but using a COP theory.

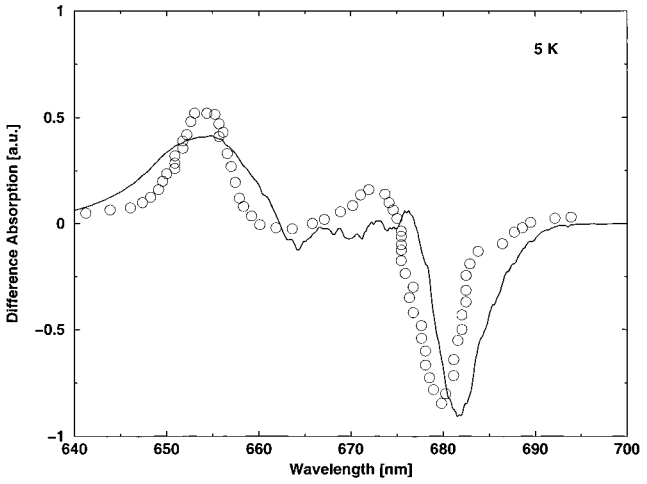

Figure 6. Calculation of linear absorption difference spectra, using a POP treatment, where the pheophytin of the D_2 branch has been replaced by a deoxo-hydroxy pheophytin, $T = 5$ K. The experimental values measured by Germano et al.[45] are shown as circles.

contributor to the blue side of the absorption spectrum between 660 and 675 nm. The difference in absorption for the two calculations, with (solid line) and without (dashed line) peripheral pigments is seen in the inset in the lower half of Figure 4.

A COP treatment (Appendix C) of the circular dichroism and linear absorption is shown in Figure 5. The mean site energy in this case is 668.5 nm, determined from the linear absorption, the inhomogeneous width is the same as in the POP calculation.

Recently, the $Pheo_{D2}$ was chemically converted to a deoxo-hydroxy pheophytin, which exhibits a 13 nm blue shift of its Q_y optical transition in solution.[45] Consequently, for the calculation of the difference spectrum in Figure 6 we shifted the mean site energy of the $Pheo_{D2}$ by 13 nm from 669 to 656 nm. The difference spectrum at 5 K, obtained from the spectrum with and without the modified $Pheo_{D2}$ is compared with the experimental results of Germano et al.[45] in Figure 6.

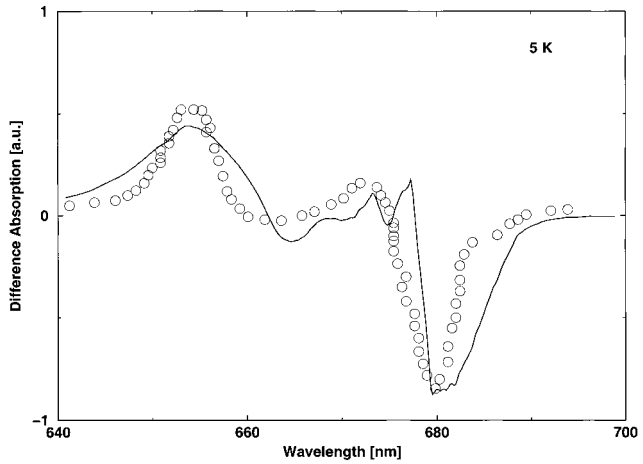

Figure 7. Same as in Figure 6 but using a COP theory.

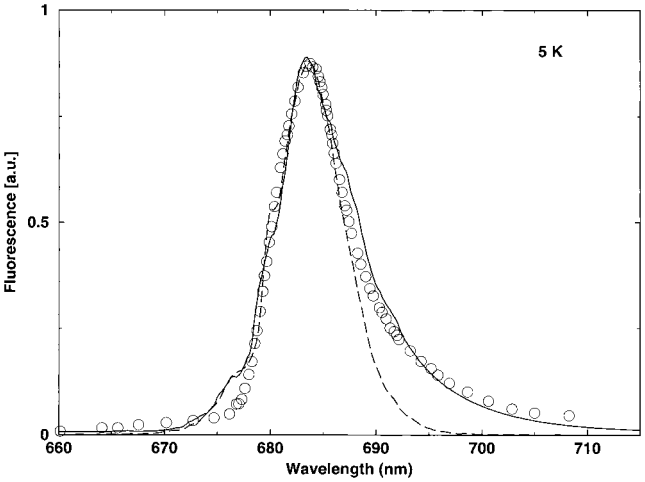

Figure 8. Calculation of 5 K fluorescence spectrum measured by Peterman et al.[33] within a non-Markovian POP theory (solid line) and a Markovian theory (dashed line).

A COP treatment (Appendix C) of the difference spectrum is shown in Figure 7.

The predicted form of the 5 K fluorescence spectrum, using eq 11 and the parameters determined above, is compared with that measured by Peterman et al.[33] in Figure 8. Also shown is the result of a calculation applying a Markov approximation. In this case a Lorentzian line shape function

$$D'_M(\omega) = \frac{(\tau'_M)^{-1}}{(\omega - \tilde{\omega}'_{M0})^2 + (\tau'_M)^{-2}} \qquad (16)$$

is obtained.[34]

A COP treatment (Appendix C) of the fluorescence is shown in Figure 9.

III. Calculations of Exciton Dynamics

A. Contributions from the Peripheral Chlorophylls. We next examine how the dephasing times of optical transitions are distributed in energy. After optical excitation, an exponential decay of occupation probabilities of exciton states $|M\rangle$ at energy $\hbar\omega_{M0}$ results when the process is Markovian. The validity of the Markov approximation for the estimation of exciton relaxation times is examined later in the calculation of pump−probe spectra.

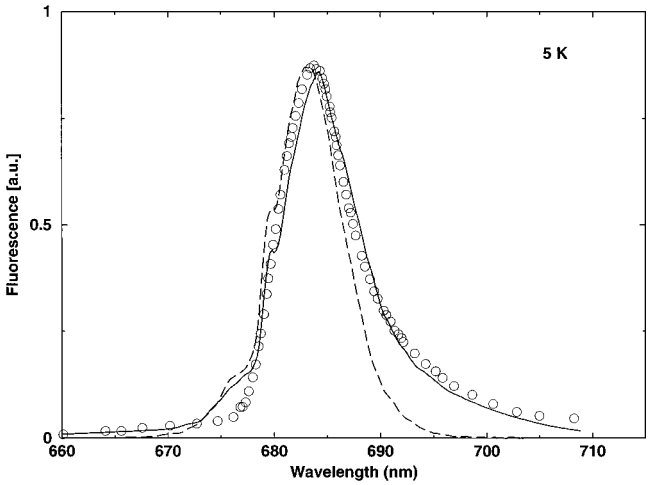

Figure 9. Same as in Figure 8 but using a COP theory.

The exciton state lifetime t_M, i.e., the decay constant of the Mth exciton state, is given by the rates $k_{M\rightarrow K}$ of exciton relaxation from this state, we have[34]

$$t_M^{-1} = \sum_K k_{M\rightarrow K} = 2\sum_K \gamma_{MK}\tilde{C}^{(Re)}(\omega_{MK}) \qquad (17)$$

In the presence of static disorder, a probability density $p_\tau(\omega)$ for the lifetime τ at any certain frequency ω can be calculated from

$$p_\tau(\omega) = \frac{\langle \sum_M \delta(\tau - t_M)\delta(\omega - \omega_{M0})\rangle_{\mathrm{dis}}}{\langle \sum_M \delta(\omega - \omega_{M0})\rangle_{\mathrm{dis}}} \qquad (18)$$

The probability $P_\omega(\tau_1,\tau_2)$ of finding at a frequency ω a lifetime τ in the interval $\tau_1 < \tau < \tau_2$ is

$$P_\omega(\tau_1,\tau_2) = \int_{\tau_1}^{\tau_2} \mathrm{d}\tau\, p_\tau(\omega) \qquad (19)$$

The probabilities obtained for the lifetimes for the PS-2 reaction center are shown in Figure 10 when the two peripheral pigments are and are not included. A major difference is seen to be the blue side of the spectrum, at wavelengths shorter than 670 nm. Specifically, some calculated lifetimes greater than 10 ps are obtained when the peripheral chlorophylls are included.

B. Calculation of Time-Resolved Pump−Probe Spectra. The 77 K pump−probe spectra have been measured by Visser et al.[22] and can be compared with results predicted from the above model. In the experiment, the sample was excited with a 400 fs pump pulse centered at 670.5 nm and the change in the absorption spectrum was probed with a delayed white probe pulse at different delay times. In the limit of fast intraexciton relaxation,[34,50] the dispersed pump−probe spectrum is given as a sum of three contributions,[34] ground-state bleaching (GB), stimulated emission (SE), and excited-state absorption (ESA):

$$\Delta\alpha_{\mathrm{disp}}(\omega) \propto \langle \mathrm{GB}(\omega) + \mathrm{SE}(\tau_{\mathrm{d}},\omega) + \mathrm{ESA}(\tau_{\mathrm{d}},\omega)\rangle_{\mathrm{dis,orient}} \qquad (20)$$

The symbol $\langle\ \rangle_{\mathrm{dis,orient}}$ denotes an average over both a static disorder of the pigments and a random orientation of pigment−protein complexes. Assuming a delta-shaped probe pulse acting at time t_{pr} is delayed by a time τ_{d} after the pump-pulse with finite width, we have[34] for nonoverlapping pulses

$$\mathrm{GB}(\omega) = -\sum_M D_M(\omega)\sum_K \rho_{KK}^{(2)}(t_{\mathrm{pr}}) \qquad (21)$$

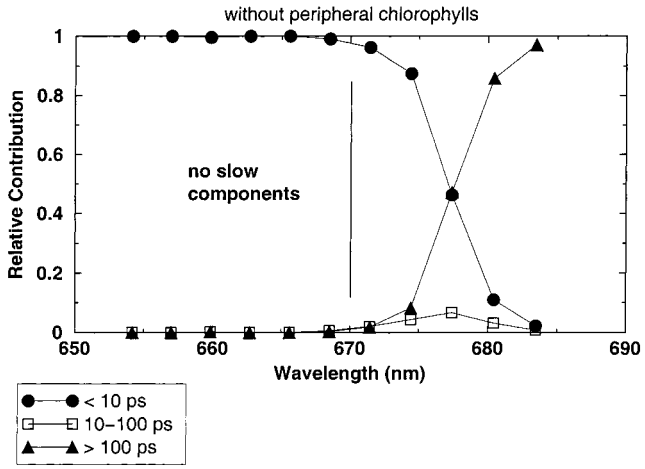

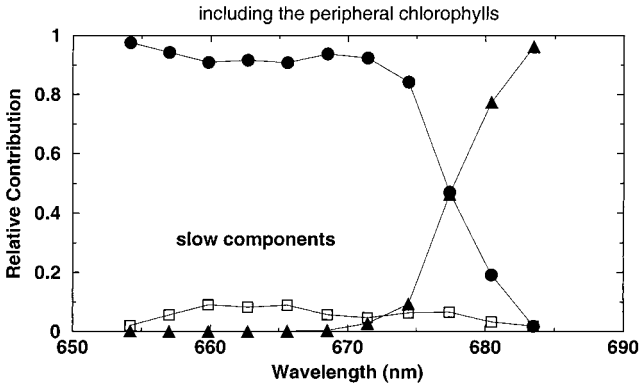

Figure 10. Dependence of exciton lifetimes on excitation wavelength and for a calculation with (upper half) and without inclusion of the peripheral pigments. The vertical line in the upper half separates the region with only fast relaxation times from a region with fast and slow times.

where $D_M(\omega)$ is the line shape function of absorption, eq 3 and $\rho_{KK}^{(2)}(t_{\mathrm{pr}})$ is the (second order) population of the Kth exciton state at time t_{pr}. The $\mathrm{SE}(\omega,\tau_{\mathrm{d}})$ is described by[34]

$$\mathrm{SE}(\omega,\tau_{\mathrm{d}}) = -\sum_M D'_M(\omega)\rho_{MM}^{(2)}(t_{\mathrm{pr}}) \qquad (22)$$

where $D'_M(\omega)$ is the fluorescence line shape function, eq 12. The $\mathrm{ESA}(\omega,\tau_{\mathrm{d}})$ is[34]

$$\mathrm{ESA}(\omega,\tau_{\mathrm{d}}) = \sum_{M,2N} D'_{M\rightarrow 2N}(\omega)\rho_{MM}^{(2)}(t_{\mathrm{pr}}) \qquad (23)$$

with the line shape function

$$D'_{M\rightarrow 2N}(\omega) = Re\int_0^\infty \mathrm{d}t\, \mathrm{e}^{i(\omega-\tilde{\omega}'_{2NM})t}\, \mathrm{e}^{G_{2NM}(t)-G_{2NM}(0)}\, \mathrm{e}^{-t/\tau_{2NM}} \qquad (24)$$

where the $\tilde{\omega}'_{2NM}$, $G_{2NM}(t)$, and τ_{2NM} are given in Appendix B.

The equations of motion for the exciton state populations $\rho_{MM}^{(2)}(t)$ are,[34] using a Markov approximation for the off-diagonal exciton-vibrational coupling as before,

$$\frac{\partial}{\partial t}\rho_{MM}^{(2)}(t) = -\frac{2}{\tau_M}\rho_{MM}^{(2)}(t) + \sum_K k_{K\rightarrow M}\rho_{KK}^{(2)}(t) + \frac{2}{\hbar}E_{\Omega_{\mathrm{pu}}}(t)\mu_M^{(\mathrm{pu})}\,\mathrm{Im}\{\mathrm{e}^{i\Omega_{\mathrm{pu}}(t)}\rho_{M0}^{(1)}(t)\} \qquad (25)$$

The dephasing constants τ_M^{-1} and rate constants $k_{M\rightarrow K}$ are those in eqs 9 and 17, respectively, $E_{\Omega_{\mathrm{pu}}}(t)$ is the pump-pulse envelope

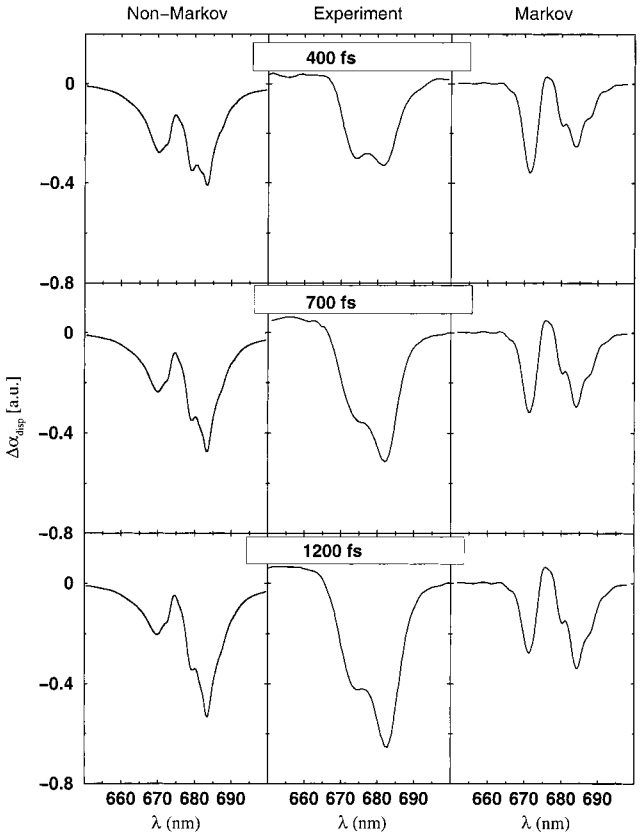

Figure 11. Calculation of 77 K pump−probe spectra for different delay times. Left column: non-Markovian POP theory. Middle: experiment by Visser et al.[22] Right: Markovian theory.

and $\mu_M^{(\mathrm{pu})}$ denotes the scalar product of the pump-pulse polarization and the optical transition dipole moment between the ground state and the Mth exciton state. The first-order density matrix elements, which enter the right side of the above equation as a source term, are obtained as[34]

$$\rho_{M0}^{(1)}(t) = \frac{i\mu_M^{(\mathrm{pr})}}{2\pi\hbar} e^{G_M(t)} \int_{-\infty}^{+\infty} d\omega \frac{e^{-i\omega t}}{\tau_M^{-1} - i(\omega - \tilde{\omega}_{M0})} \int_0^{+\infty} d\tau \times e^{i(\omega-\Omega_{\mathrm{pu}})\tau} e^{-G_M(\tau)} E_{\Omega_{\mathrm{pu}}}(\tau) \quad (26)$$

where $\mu_M^{(\mathrm{pr})}$ is the scalar product with the probe pulse polarization.

For the calculation of the pump−probe spectra, a 400 fs pump-pulse as in the experiment was assumed and the probe pulse was modeled by a delta-shaped pulse, instead of random generation of 400 fs probe pulses with different carrier frequencies as in the experiment. The calculated 77 K pump−probe spectra are compared with experiment and with a Markovian treatment in Figure 11 for different delay times, assuming a correlation radius of protein vibrations of $R_c = 5$ Å. A comparison of the present POP and alternative COP calculations of the pump−probe spectra is given in Appendix C.

IV. Discussion

A. The Redistribution of Oscillator Strengths by the Excitonic Coupling in the Linear Absorption Spectrum. One aim of this paper is to investigate different mechanisms that might be responsible for the observed multiexponential exciton relaxation in the PS-2 reaction center. Qualitative information on the heterogeneous nature of the system is obtained from the fit of the absorption spectrum. As seen in the lower half of Figure 4, the major contribution from the two peripheral chlorophylls to the absorption spectrum occurs on the blue side of the spectrum. The oscillator strength of the two peripheral chlorophylls remains around 670 nm, due to the weak excitonic coupling, whereas the strong interaction between the six core pigments leads to enhanced oscillator strengths of the exciton states in the red part of the spectrum. It has been inferred[27] from linear absorption and transient absorption spectra of different preparations of PS-2 reaction center samples, containing one or two peripheral pigments that the peripheral pigments absorb at 670 nm. The present assignment of the mean site energy for the pigments agrees with that inference. On the basis of hole burning experiments, it had been suggested, instead, that the peripheral chlorophyll in the D_1 branch might absorb at 684 nm.[52] A suitable mutation experiment would be helpful to clarify this point. The interpretation of such an experiment would be simplified by the fact that the weak coupling of the peripheral chlorophylls and six core pigments allows an assignment of the mean site energy of the peripheral chlorophylls directly from the difference absorption spectrum (Figure 4 inset).

B. The Contribution from *Pheo*$_{D2}$ to the Optical Absorption Revealed in the Absorption Difference Spectra. When the contribution to the linear absorption spectrum of one of the core pigments is missing, the interpretation of the difference spectra becomes more complex, as seen for the *Pheo*$_{D2}$ in Figure 6, where the calculation of the measured absorption difference spectra[45] at 5 K is shown. The pheophytin of the D_2 branch has been replaced by a deoxo-hydroxy pheophytin, which is known from measurements in solution to absorb 13 nm to the blue of the unmodified pheophytin.[45] Therefore, for the calculation of the difference spectrum we shifted the mean site energy of *Pheo*$_{D2}$ from 669 to 656 nm. The calculated and measured spectra agree well, a positive peak around 655 nm appearing because of the absorption of the modified *Pheo*$_{D2}$.[53] In both the experimental and calculated spectra, a single negative peak occurs around 680 nm and reflects the contribution of the unmodified *Pheo*$_{D2}$ to an exciton transition at this wavelength.

From measurements on reduced *Pheo*$_{D2}$ it was suggested[54] that this pigment would contribute mostly at 669 nm to the absorption spectrum, an assignment which differs from a more recent assignment.[45] The agreement of the present calculation with the experimental data[45] indicates that indeed the *Pheo*$_{D2}$ contributes most to an exciton transition around 680 nm and therefore that electrochromic effects should be taken into account for an interpretation of the difference absorption spectra measured[54] on PS-2 reaction centers with reduced *Pheo*$_{D2}$.

C. The Vibrational Sidebands in the Fluorescence Spectrum and a Comparison of POP and COP. Further evidence for the predictive power of the present simple model is obtained from the calculation of the fluorescence spectra measured by Peterman et al. at 5 K.[33] The non-Markovian calculation is shown in Figure 8 and compared with a Markovian calculation. Both calculated spectra agree qualitatively with experiment around the fluorescence maximum at 683.8 nm. The non-Markovian theory, however, allows one to describe also the low-energy side of the spectrum, whereas the Markovian theory gives a large discrepancy in this region. This difference is due the inclusion of the vibrational sidebands in the non-Markovian theory.

An alternative COP treatment (Appendix C) of the fluorescence is shown in Figure 9. It is interesting to note that both non-Markovian theories, the POP in Figure 8 and the COP in Figure 9, describe the experiment equally well. It was found elsewhere[34] that the POP theory gives a better description of

the homogeneous vibrational sideband measured in fluorescence line narrowing spectra of B820 complexes, whereas the COP fails to describe the low-energy part of the sideband, the reason being the exact summation of the diagonal part of the exciton-vibrational coupling in POP and the inexact partial summation in COP. However, as far as inhomogeneous spectra are concerned, the involved disorder average leads to very similar results in POP and COP. This similarity is seen also in the circular dichroism and linear absorption by comparing the POP results in Figure 4 with the COP results in Figure 5, in the simulation of absorption difference spectra in Figures 6 and 7, and in the calculation of pump−probe spectra in Appendix C. We note that in a Markovian limit the POP and COP line shape functions reduce to identical Lorentzian forms.[55]

The high-energy shoulder occurring in the theoretical fluorescence spectra in Figures 8 and 9 around 675 nm is not seen in the experiment. It presumably arises from the distribution function of the energy of the lowest exciton state. In that case the assumption of independent Gaussian distributed site energies would be too simple.

D. Dynamics, Hole Burning and Pump−Probe Spectra. Since the coupling between the peripheral chlorophylls and the core pigments is weak, lifetimes greater than 10 ps are predicted at short wavelengths, where the peripheral pigments absorb. This result is seen in the lower half of Figure 10. From pump−probe experiments it has been proposed[25−27] that the peripheral pigments give rise to such long exciton relaxation times, in agreement with the present calculated lifetimes. We note that in the absence of the peripheral pigments no long lifetimes are obtained for the blue side of the spectrum, as seen in the upper half of Figure 10. This fact rules out static disorder among the six core pigments as a possible source for long exciton relaxation times.

In addition, as will be seen in the discussion of the pump−probe spectra the inclusion of non-Markovian contributions yields a similar time scale for exciton relaxation. We conclude, therefore, that the heterogeneity in pigment couplings due to the two peripheral chlorophylls serves to explain the observed picosecond transfer times found in hole burning in the blue side of the spectrum. To detect the fast component there might be difficult, because of the relatively low oscillator strength of the six core pigments in this region. In addition, there is an inherently higher sensitivity of hole burning experiments for the detection of longer lifetimes, since a conformational change of the protein during the excited state lifetime of the pigment is needed for the observation. We note that the calculated increase in lifetimes at the red end of the spectrum in Figure 10 is due to the lowest exciton state, since it can only lose its population by thermal activation and the latter is small at 5 K.

A fast subpicosecond exciton relaxation is seen in the calculation of pump−probe spectra in Figure 11. Despite a major discrepancy between the calculated and measured spectra around 675 nm, qualitatively similar behavior in experiment and theory is obtained. Namely, the low-energy peak around 683 nm rises with increasing delay time (from top to bottom in Figure 11) relative to the high-energy peak. The latter peak occurs at 670 nm in the calculations and at 673 nm in the experiment.

Due to relaxation from the states around 670 nm, where the pump-pulse excites the upper exciton states, to the low-energy states, the stimulated emission from these states leads to a rise of the magnitude of the peak around 680 nm. Since the oscillator strength of the six core pigments is smaller in the 670 nm region than in the low-energy side of the spectrum (as seen, for example, in absorption in the lower half of Figure 4), the stimulated emission in the low-energy side is stronger than at higher energies and therefore the increase of the peak at 680 nm is larger than the decay of the peak at 670 nm. A major part of the stimulated emission at 670 nm stays at this wavelength, because it originates from the two peripheral chlorophylls, which exhibit a relaxation dynamics on a 10 ps and longer (as shown in Figure 10) time scale.

In addition to the spectral difference around 675 nm in theory and experiment, an increased magnitude of the whole spectrum is obtained with increased delay time in the experiment. The data that are linear in the coupling to the external field, namely in Figures 4, 6, and 8, agree better with experiment than do the pump−probe data (Figure 11), which are of third-order in the external field. A possible reason for this difference might be the neglect of doubly excited pigment states[56−58] affecting the excited-state absorption, which is of third order in the external field and so influences the pump−probe spectra. The interpretation of both types of experiments also depends on the input data (intermolecular couplings and optical transition dipoles). It is perhaps not surprising therefore, that the discrepancies between theory and experiment are smaller in the linear spectra and are amplified in the nonlinear optical spectra.

The Markovian calculation of the pump−probe spectra shown in the right column of Figure 11 yields larger discrepancies than the non-Markovian (in the left column) with the experimental results because of the neglect of the vibrational sidebands of optical transitions. The latter was discussed before in the calculation of the fluorescence in Figure 8. The calculations of the pump−probe spectra obtained with a COP theory are compared in Appendix C (Figure 12) to the POP treatment used in Figure 11. Very similar behavior is obtained in the POP and COP theories, in particular the relative rise of the 680 nm peak occurs on the same time scale. The temporal behavior of the spectra is determined by the off-diagonal parts of the exciton vibrational coupling, which is responsible for exciton relaxation. The COP theory treats the whole exciton-vibrational coupling as non-Markovian, whereas the POP theory uses a Markovian theory for the off-diagonal part of the coupling. The similar relaxation dynamics obtained in both theories rules out non-Markovian effects as major contributors to the multiexponential exciton relaxation measured in PS-2 reaction centers on the time scale of greater than 400 fs. Non-Markovian contributions to exciton relaxation can be expected for delay times smaller than 100 fs, which is the estimated[34] decay constant of the correlation function of the pigment's transition energies.

E. General Remarks. The present simple model provides an interpretation of the various frequency domain linear optical spectra (linear absorption, fluorescence, absorption difference) and the time-dependence of pump−probe spectra in terms of multiexponential exciton relaxation. Two parameters were extracted from the CD results, namely, (i) the mean site energy of the pigments corresponding to 669 nm, assumed to be equal for all pigments, and (ii) the inhomogeneous width for the distribution of the pigment's transition energies, $\Delta_{dis} = 300\ cm^{-1}$. A third parameter, the correlation radius of protein vibrations $R_c = 5$ Å, was estimated from pump−probe spectra. As was noted earlier, the linear spectra are relatively insensitive to R_c.

Although there are quantitative differences between the theory and the experiment, the various spectra are qualitatively similar. Any quantitative difference may have several origins, e.g., the assumption of the same site energy for all pigments, the assumption of a single correlation radius for all protein vibrations,[59] or the lack of current knowledge of the correct dipole geometries. In this respect we investigated how the

spectra change upon independent 90 degree rotation of the transition dipole moments of the six core pigments. The linear absorption and circular dichroism spectra for all $2^6 = 64$ possible such transition dipole configurations were simulated. For a few of them, even within the minimal model of same site energies, the quantitative agreement with the experiment could be increased.

Until higher resolution structural studies become available, the dipole configuration suggested in Svensson's structural model[8] was assumed instead. From high field electron paramagnetic resonance measurements[61] and density functional calculations[62] on the pheophytin radical of the D_1 branch, evidence was obtained that the $Pheo_{D1}$ has the same orientation as the bacteriopheophytin in the bacterial reaction center. This assignment is in agreement with the one given in Svensson's structural model.[8] Very recently, additional support of the present assignment of optical transition dipoles was given in ref 63.

V. Summary

The present model offers an explanation for the discrepancy of a factor of 100 between the different relaxation times observed in experiments on the PS-2 reaction center. The subpicosecond relaxation results from exciton relaxation among the six strongly interacting core pigments of the complex. The observed exciton relaxation from high-energy exciton states with time scales larger than 10 ps is likely to occur between the two peripheral pigments and the six core pigments.

The present study indicates that the coupling between the six core pigments in the PS-2 reaction center redistributes the oscillator strengths of the pigments toward the red-shifted exciton states. The excited states of the two peripheral chlorophylls are strongly localized and almost unshifted in energy. These two aspects lie at the heart of the present explanation of the striking deviation in transfer times measured in the PS-2 reaction center.

In the bacterial reaction center the red shift of the lowest exciton state with respect to the exciton states of the surrounding antennae is larger because of the stronger coupling within the special pair. Hence, a possible reason for the change in the distance between the special pair pigments that occurred in evolution may be the postulated[64] need for a shallow trap for the excitation energy.

The present study represents a first step in the direction of a more microscopic understanding of exciton relaxation in the PS-2 reaction center. Fluorescence line narrowing, circular dichroism spectra, and pump−probe spectra were used to make predictions for linear absorption, absorption difference, and fluorescence data. The results showed reasonable agreement with the data. A refinement of the model presented here and an inclusion of electron transfer into the theory awaits more elaborate expressions for the interaction energy of the pigments, as well as higher resolution structural data and further optical experiments. In the latter context, mutation studies and low-temperature pump−probe spectra with a higher time-resolution would be of interest.

Acknowledgment. We would like to acknowledge support of a Lynen Research Fellowship from the Alexander von Humboldt Foundation to one of us (T.R.). The support of the National Science Foundation and the Office of Naval Research is also appreciated. We thank Prof. A. Holzwarth and Dr. V. Prokhorenko for bringing the exciton vibrational dynamics in the PS-2 reaction center to our attention, and thank Dr. M. Hodoscek for preparing Figure 2. We also thank Prof. G. Small and Dr. R. Jankowiak for helpful comments.

Appendix A: Scheme for the Extraction of the Spectral Density

The spectral density $J(\omega)$ has been extracted elsewhere[34] from fluorescence line narrowing spectra of B777 complexes.[35] The dependence of the fluorescence spectrum on the excitation energy $\hbar\omega_{exc}$ is[34]

$$I(\omega,\omega_{exc}) \sim e^{-2G(0)}P_{inh}(\omega_{exc} - \bar{\omega}_{10})\delta(\omega - \omega_{exc}) + e^{-G(0)}(P_{inh}(\omega_{exc} - \bar{\omega}_{10}) + P_{inh}(\omega - \bar{\omega}_{10}))\phi(\omega_{exc} - \omega) + \int d\omega_{10}\, P_{inh}(\omega_{10} - \bar{\omega}_{10})\phi(\omega_{10} - \omega)\phi(\omega_{exc} - \omega_{10}) \quad (A1)$$

where

$$\phi(\omega) = \frac{e^{-G(0)}}{2\pi}\int_{-\infty}^{\infty} dt\, e^{i\omega t}\{e^{G(t)} - 1\} \quad (A2)$$

and the time-dependent function $G(t)$ is related to the spectral density $J(\omega)$ according to

$$G(t) = \int_{-\infty}^{\infty} d\omega\, e^{i\omega t}(1 + n(\omega))(J(\omega) - J(-\omega)) \quad (A3)$$

A Gaussian distribution function P_{inh} for the site energy of the pigment was assumed centered at the mean site energy $\hbar\bar{\omega}_{10}$. The following functional form of the spectral density was assumed

$$J(\omega) = \sum_{i=1,2} s_i \frac{p}{\omega_i^{(q+1)}\Gamma((q+1)/p)}\omega^q e^{-(\omega/\omega_i)^p} \quad (A4)$$

As an initial guess for the spectral density, the shape of the vibrational sideband at the lowest excitation energy and an amplitude $s_1 + s_2 = 1$ common for photosynthetic pigment−protein complexes were chosen. The fit of eq A1 to the experiment was iteratively completed by performing the two Fourier transforms eqs A2 and A3. The optimized parameters are given in the present text. Further details on the extraction of the spectral density are given in ref 34.

Appendix B: Functions for the ESA Lineshape Function

The frequencies $\tilde{\omega}'_{2NM}$ are

$$\tilde{\omega}'_{2NM} = \omega'_{2NM} - \frac{E_\lambda}{\hbar}(\gamma_{2N2N} + \gamma_{MM} - 2\gamma_{2N2NMM}) + \sum_{2K}(1 - \delta_{2K2N})\gamma_{2N2K}\tilde{C}^{(Im)}(\omega'_{2N2K}) + \sum_{K}(1 - \delta_{KM})\gamma_{KM}(\tilde{C}^{(Im)}(\omega'_{MK}))^* \quad (B1)$$

where in addition to the one-exciton functions γ_{MK} in eq 6, a two-exciton function γ_{2N2M}

$$\gamma_{2N2M} = \sum_{m>n}\sum_{k>l} c_{mn}^{(2N)}c_{mn}^{(2M)}c_{kl}^{(2N)}c_{kl}^{(2M)} \times (e^{-R_{mk}/R_c} + e^{-R_{ml}/R_c} + e^{-R_{nk}/R_c} + e^{-R_{nl}/R_c}) \quad (B2)$$

with $M = N$ and a mixed function γ_{2N2NMM}

$$\gamma_{2N2NMM} = \sum_{m>n}\sum_{k}(c_{mn}^{(2N)})^2(c_k^{(M)})^2(e^{-R_{mk}/R_c} + e^{-R_{nk}/R_c}) \quad (B3)$$

were used and we have

$$\omega'_{2NM} = \omega'_{2N0} - \omega'_{M0} \quad (B4)$$

with the ω'_{M0} in eq 15 and

$$\omega'_{2N0} = \omega_{2N0} - 2\gamma_{2N2NMM}E_\lambda/\hbar \tag{B5}$$

where $\omega_{2K0} = \epsilon_{2K}/\hbar$ is a two-exciton eigenfrequency.

The time-dependent function $G_{2NM}(t)$ is

$$G_{2NM}(t) = (\gamma_{2N2N} + \gamma_{MM} - 2\gamma_{2N2NMM})\int_{-\infty}^{\infty} d\omega \times e^{-i\omega t}\{(1 + n(\omega))J(\omega) + n(-\omega)J(-\omega)\} \tag{B6}$$

The inverse dephasing time $\tau_{2NM}^{-1} = \tau_{2N}^{-1} + \tau_M^{-1}$ contains the one-exciton dephasing constant in eq 9 and τ_{2N}^{-1} is the two-exciton constant

$$\tau_{2N}^{-1} = \sum_{2K}\gamma_{2N2K}\tilde{C}^{(Re)}(\omega'_{2N2K}) \tag{B7}$$

where $\omega'_{2N2K} = \omega'_{2N0} - \omega'_{2K0}$.

Further details can be found in ref 34.

Appendix C: Calculation of Optical Spectra Using the COP Formalism

1. Linear Optical Spectra. Within a COP formalism the line shape functions $D_M(\omega)$ for absorption and circular dichroism and $D'_M(\omega)$ for fluorescence in eqs 1, 2, and 11 are obtained as[34,40]

$$D_M(\omega) = \mathrm{Im}\left\{\frac{1}{\omega_{M0} - \omega - i\Gamma_M(\omega)}\right\}$$

and

$$D'_M(\omega) = \mathrm{Im}\left\{\frac{1}{\omega'_{M0} - \omega - i\Gamma'_M(\omega)}\right\} \tag{C1}$$

where the $\Gamma_M(\omega)$ function is defined by

$$\Gamma_M(\omega) = \sum_K \gamma_{MK}\tilde{C}(\omega - \omega_{K0}) \tag{C2}$$

and $\Gamma'_M(\omega)$ is

$$\Gamma'_M(\omega) = \sum_K (1 - \delta_{MK})\gamma_{MK}\tilde{C}(\omega - \omega'_{K0}) + \gamma_{MM}\tilde{C}^*(\omega'_{M0} - \omega) \tag{C3}$$

with the $\tilde{C}(\omega)$ in eq 7. The Markovian limit is obtained by setting $\Gamma_M(\omega) = \Gamma_M(\omega_{M0})$ and $\Gamma'_M(\omega) = \Gamma'_M(\omega'_{M0})$. Within this limit the POP and COP equations become identical.

The linear optical spectra obtained using the above line shape functions are shown in Figures 5, 7, and 9.

2. Pump−Probe Spectra. For the calculation of pump−probe spectra, a non-Markovian solution for the second-order exciton state populations $\rho^{(2)}_{MM}(t)$ is obtained from

$$\rho^{(2)}_{MM}(t) = P^{(eq)}_M + \Delta P_M(t) \tag{C4}$$

where $P^{(eq)}_M$ is the equilibrium population

$$P^{(eq)}_M = \sigma^{(eq)}_{MM} = \frac{e^{-\hbar\omega_{M0}/kT}}{\sum_N e^{-\hbar\omega_{N0}/kT}}\sum_K \tilde{\jmath}^{(2)}_{KK}(\omega = 0) \tag{C5}$$

and $\Delta P_M(t)$ is the inverse Fourier transform of $\Delta\tilde{P}_M(\omega)$, for which the following set of linear equations is solved in the frequency domain[34]

$$-i\omega\Delta\tilde{P}_M(\omega) + \sum_N \gamma_{MN}\{(\tilde{C}(\omega_{MN} + \omega) + \tilde{C}^*(\omega_{MN} - \omega))\Delta\tilde{P}_M(\omega) - (\tilde{C}(\omega_{NM} + \omega) + \tilde{C}^*(\omega_{NM} - \omega))\Delta\tilde{P}_N(\omega)\} = -P^{(eq)}_M + \frac{i}{\omega}P^{(eq)}_M\sum_N \gamma_{MN}([\tilde{C}(\omega_{MN} + \omega) + \tilde{C}^*(\omega_{MN} - \omega)] - e^{-\hbar\omega_{NM}/kT}[\tilde{C}(\omega_{NM} + \omega) + \tilde{C}^*(\omega_{MN} - \omega)]) + \tilde{\jmath}^{(2)}_{MM}(\omega) \tag{C6}$$

where $\tilde{\jmath}^{(2)}_{MM}(\omega)$ in eqs C5 and C6 is the Fourier−Laplace transform of

$$\jmath^{(2)}_{MM}(t) = \frac{2}{\hbar}\mu^{(pu)}_M \mathrm{Im}(e^{i\Omega_{pu}t}\rho^{(1)}_{M0}(t)) \tag{C7}$$

The $\mu^{(pu)}_M$ term denotes a scalar product of the optical transition dipole of the transition between the ground state and the Mth exciton state and the pump-pulse polarization, and $\rho^{(1)}_{M0}(t)$ is obtained from an inverse Fourier transform of $\tilde{\rho}^{(1)}_{M0}(\omega)$:

$$\hbar\tilde{\rho}^{(1)}_{M0}(\omega) = -\frac{\mu^{(pu)}_M\tilde{E}_{\Omega_{pu}}(\omega - \Omega_{pu})}{\omega - \omega_{M0} + i\Gamma_M(\omega)} \tag{C8}$$

where the Γ_M function in eq C2 was used and $\tilde{E}_{\Omega_{pu}}(\omega - \Omega_{pu})$ is the transform of the pump pulse envelope $E_{\Omega_{pu}}(t)$.

The pump−probe spectra then follow from eqs 20 and 21−23, using the line shape functions in eq C1 for ground-state bleaching and stimulated emission. The ESA line shape function $D_{M\rightarrow 2N}(\omega)$, using COP, is[34]

$$D_{M\rightarrow 2N}(\omega) = -(\mu^{(pr)}_{M\rightarrow 2N})^2\,\mathrm{Im}\left(\frac{1}{\omega - \omega'_{2NM} + i\Gamma'_{2N}(\omega)}\right) \tag{C9}$$

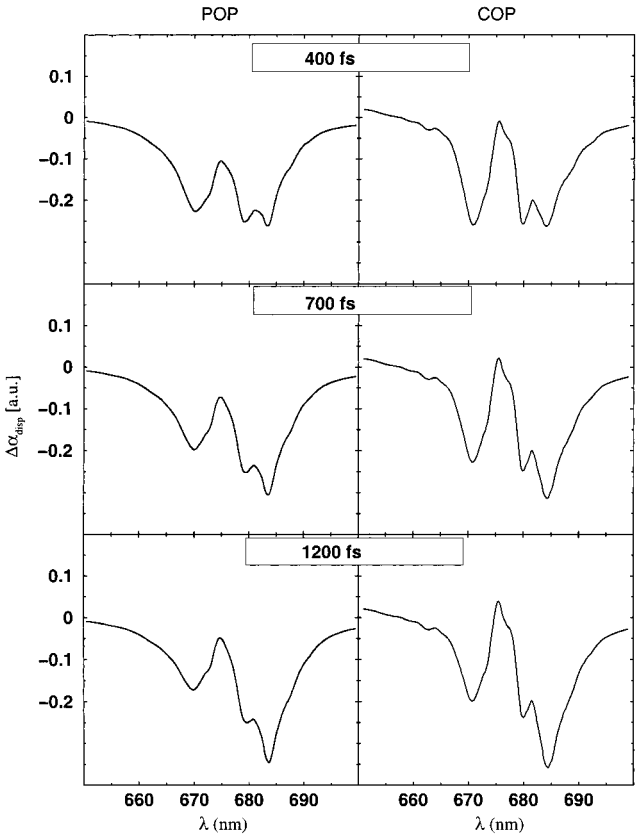

Figure 12. Comparison of 77 K pump−probe spectra calculated in POP formalism (left half) and COP formalism (right half).

with the damping function $\Gamma'_{2N}(\omega)$

$$\Gamma'_{2N}(\omega) = \sum_{2K}(1-\delta_{2N2K})\gamma_{2N2K}\tilde{C}(\omega-\omega'_{2KM}) + \sum_{K}(1-\delta_{MK})\gamma_{MK}\tilde{C}(\omega'_{2NK}-\omega) + (\gamma_{2N2N}+\gamma_{MM}-2\gamma_{2N2NMM})C(\omega) \quad \text{(C10)}$$

where the different γ functions and the frequency ω'_{2NM} are given in Appendix B and eq 6.

The pump−probe spectra obtained from the above equations are compared in Figure 12 to spectra obtained using a POP treatment. The correlation radius was chosen as $R_c = 7$ Å, the mean site energy and inhomogeneous width were chosen as in the linear spectra, a 400 fs pump-pulse centered at 670.5 nm and a delta shaped probe pulse were used.

Note Added after ASAP Posting

This article was released ASAP on 1/30/2002 with an error in eq 16. The correct version was posted 2/14/2002.

References and Notes

(1) Rhee, K.-H.; Morris, E. P.; Barber, J.; Kühlbrandt, W. *Nature* **1998**, *396*, 283.

(2) Zouni, A.; Witt, H. T.; Kern, J.; Fromme, P.; Krauss, N.; Saenger, W.; Orth, P. *Nature* **2001**, *409*, 739.

(3) Deisenhofer, J.; Epp, O.; Miki, K.; Huber, R.; Michel, H. *Nature* **1985**, *318*, 618.

(4) Michel, H.; Deisenhofer, J. *Biochemistry* **1988**, *27*, 1.

(5) Tetenkin, T.; Gulyaev, B. A.; Seibert, M.; Rubin, A. B. *FEBS Lett.* **1989**, *250*(2), 459.

(6) Braun, P.; Greenberg, M.; Scherz, A. *Biochemistry* **1990**, *29*, 10376.

(7) Kwa, S.; Eijckelhoff, C.; van Grondelle, R.; Dekker, J. P. *J. Phys. Chem.* **1994**, *98*, 7702.

(8) Svensson, B.; Etchebest, C.; Tuffery, P.; van Kann, P. J.; Smith, J.; Styring, S. *Biochemistry* **1996**, *35*, 14486. Svensson, B; van Kann, P. J., Styring, S. *In Photosynthesis: From Light to Biosphere*; Mathis, P., Ed.; Kluwer Academic Publishers: Dordecht, The Netherlands, 1955; p 425.

(9) Xiong, J.; Subramaniam, S.; Govindjee *Photosynth. Res.* **1998**, *56*, 229.

(10) van Brederode, M. E.; van Grondelle, R. *FEBS Lett.* **1999**, *455*, 1.

(11) Hankamer, B.; Morris, E. P.; Barber, J. *Nature Struct. Biol.* **1999**, *6*, 560.

(12) Thompson, L. K.; Brudvig, G. W. *Biochemistry* **1988**, *27*, 6653.

(13) Dekker, J. P.; Van Grondelle, R. *Photosynth. Res.* **2000**, *63*, 195.

(14) Shkuropatov, A. Y.; Khatypov, R. A.; Volshchukova, T. S.; Shkuropatova, V. A.; Owens, T. G.; Shuvalov, V. A. *FEBS Lett.* **1997**, *420*, 171.

(15) Shkuropatov, A. Y.; Khatypov, R. A.; Shkuropatova, V. A.; Zvereva, M. G.; Owens, T. G.; Shuvalov, V. A. *FEBS Lett.* **1999**, *450*, 163.

(16) Prokhorenko, V.; Holzwarth, A. R. *J. Phys. Chem. B* **2000**, *104*, 11563.

(17) From transient hole burning studies at 4 K an electron-transfer time of 1.9 ps was estimated.[18] Latest transient absorption measurements yield a 7 ps and a slower 50 ps transfer time for the primary electron transfer.[19] The simulation[16] of photon echo experiments[16] revealed a distribution of effective charge-transfer times ranging from 1.5 ps to a few nanoseconds.

(18) Jankowiak, R.; Tang, D.; Small, G. J.; Seibert M. *J. Phys. Chem.* **1989**, *93*, 1649.

(19) Greenfield, S. R.; Seibert, M.; Govindjee; Wasielewski, M. R. *J. Phys. Chem. B* **1997**, *101*, 2251.

(20) Tang, D.; Jankowiak, R.; Seibert, M.; Yocum, C. F.; Small, G. J. *J. Phys. Chem.* **1990**, *94*, 6519.

(21) Durrant, J. R.; Hastings, G. H.; Joseph, D. M.; Barber, J.; Porter, G.; Klug, D. R. *Proc. Natl. Acad. Sci. U.S.A.* **1992**, *89*, 11632.

(22) Visser, H. M.; Groot, M. L.; van Mourik, F.; van Stokkum, I. H. M.; Dekker, J. P.; van Grondelle, R. *J. Phys. Chem.* **1995**, *99*, 15304.

(23) Klug, D. R.; Durrant, J. R.; Barber, J. *Philos. Trans. R. Soc. London, Ser. A* **1998**, *356*, 449.

(24) Roelofs, T. A.; Gilbert, M.; Shuvalov, V. A.; Holzwarth, A. R. *Biochim. Biophys. Acta* **1991**, *1060*, 237.

(25) Rech, T.; Durrant, J. R.; Joseph, D. M.; Barber, J.; Porter, G.; Klug, D. R. *Biochemistry* **1994**, *33*, 14768.

(26) Schelvis, J. P. M.; van Noort, P. I.; Aartsma, T. J.; van Gorkom, H. J. *Biochim. Biophys. Acta* **1994**, *1184*, 242.

(27) Vacha, F.; Joseph, D. M.; Durrant, J. R.; Telfer, A.; Klug, D. R.; Porter, G.; Barber, J. *Proc. Natl. Acad. Sci. U.S.A.* **1995**, *92*, 2929.

(28) Durrant, J. R.; Klug, D. R.; Kwa, L. S.; van Grondelle, R.; Porter, G.; Dekker, J. P. *Proc. Natl. Acad. Sci. U.S.A.* **1995**, *92*, 4798.

(29) Leegwater, J. A.; Durrant, J. R.; Klug, D. R. *J. Phys. Chem. B* **1997**, *101*, 7205.

(30) Fidder, H.; Knoester, J.; Wiersma, D. A. *J. Chem. Phys.* **1993**, *98*, 6564.

(31) Renger, T., May, V.; Kühn, O. *Phys. Rep.* **2001**, *343*, 138.

(32) May, V.; Kühn, O. *Charge and Energy Transfer Dynamics in Molecular Systems: A Theoretical Introduction*; Wiley, VCH: Berlin, 2000; pp 293, 389.

(33) Peterman, E. J. G.; van Amerongen, H.; van Grondelle, R.; Decker, J. P. *Proc. Natl. Acad. Sci. U.S.A.* **1998**, *95*, 6128.

(34) Renger T.; Marcus, R. A. *J. Chem. Phys.*, submitted.

(35) Creemers, T. M. H.; De Caro, C. A.; Visschers, R. W.; van Grondelle, R.; Völker, S. *J. Phys. Chem. B* **1999**, *103*, 9770.

(36) Kubo, R. *J. Math. Phys.* **1963**, *4*, 174.

(37) van Kampen, N. G. *Physica* **1974**, *74*, 215, 239.

(38) Hashitsume, N.; Shibata, F.; Shingu, M. *J. Stat. Phys.* **1977**, *17*, 155.

(39) Mukamel, S.; Oppenheim, I.; Ross, J. *Phys. Rev. A* **1978**, *17*, 17.

(40) Renger, T.; May, V. *Phys. Rev. Lett.* **2000**, *84*, 5228.

(41) Konermann, L.; Holzwarth, A. R. *Biochemistry* **1996**, *35*, 829.

(42) Lax, M. *J. Chem. Phys.* **1952**, *20*, 1752.

(43) Kubo, R.; Toyozawa, Y. *Prog. Theor. Phys.* **1955**, *13*, 160.

(44) Pullerits, T.; Monshouwer, R.; van Mourik, F.; van Grondelle, R. *Chem. Phys.* **1995**, *194*, 395.

(45) Germano, M.; Shkuropatov, A. Y.; Permentier, H.; Khatypov, R. A.; Shuvalov, V. A.; Hoff, A. J.; van Gorkum, H. J. *Photosynth. Res.* **2000**, *64*, 189.

(46) Cory, M. G.; Zerner, M. C.; Hu, X.; Schulten, K. *J. Phys. Chem. B* **1998**, *102*, 7640.

(47) Krueger, B. P.; Scholes, G. D.; Fleming, G. R. *J. Chem. Phys. B* **1998**, *102*, 5378.

(48) Tretiak, S.; Middleton, C.; Chernyak, V.; Mukamel, S. *J. Phys. Chem. B* **2000**, *104*, 4519.

(49) Hsu C. P.; Fleming G. R.; Head-Gordon, M.; Head-Gordon, T. *J. Chem. Phys.* **2001**, *114*, 3065.

(50) This approximation assumes that the vibrational relaxation in the excitonic potential energy surfaces[34] is fast and neglects certain coherent contributions (e.g., ref 51) to the pump−probe signal.

(51) Mukamel, S. *Principles of Nonlinear Optical Spectroscopy*; Oxford University Press: New York, 1995; p 151.

(52) Chang, H.-C.; Jankowiak, R.; Reddy, N. R. S.; Yocum, C. F.; Picorel, R.; Seibert, M.; Small, G. J. *J. Phys. Chem.* **1994**, *98*, 7725.

(53) The fact that the positive peak at 655 nm occurs close to the mean site energy of the modified $Pheo_{D2}$, 656 nm, indicates that this state is localized at the $Pheo_{D2}$. Otherwise, a further shift by the excitonic coupling would have resulted.

(54) Jankowiak, R.; Rätsep, M.; Picorel, R.; Seibert, M.; Small, G. J. *J. Phys. Chem. B* **1999**, *103*, 9759.

(55) The Markovian curves in Figures 8 and 9 are identical except for a 0.5 nm shift of the COP curve to shorter wavelengths resulting from the 0.5 nm difference in site energies in the two calculations.

(56) Leupold, D.; Mory, S.; König, R.; Hoffmann, P.; Hieke, B. *Chem. Phys. Lett.* **1977**, *45*, 567.

(57) Shepanski, J. F.; Anderson, R. W. *Chem. Phys. Lett.* **1981**, *78*, 165.

(58) Oksanen, J. A. I.; Martinsson, P.; Akesson, E.; Hynninen, P. H.; Sundström, V. *J. Phys. Chem. A* **1998**, *102*, 4328.

(59) More structural parameters than just the spatial distance between the two pigments may be important. The correlation radius is likely to to be a function of the frequency of the normal modes, since high-frequency modes can be expected to be more localized.

(60) (a) The electron density of the porphyrins in ref 2 did allow the resolution of the planes of the porphyrins. However, only little structure could be resolved inside the plain, the asymmetry for the electron density of the two pheophytins being somewhat greater than for the rest of the pigments. Therefore, there is no direct structural information available yet on the geometry of optical transition dipoles (P. Fromme, private communication). (b) A 180° rotation of any transition dipole would not change the optical spectra calculated here, but would lead to some sign changes in Table 1.

(61) Dorlet, P.; Rutherford, A. W.; Un, S. *Biochemistry* **2000**, *39*, 7826.

(62) Dorlet, P.; Xiong, L.; Sayre, R. T.; Un, S. *J. Biol. Chem.* **2001**, *276*, 22313.

(63) Vasil'ev, S.; Orth, P.; Zouni, A.; Owens, T. G.; Bruce, D. *Proc. Natl. Acad. Sci. U.S.A.* **2001**, *98*, 8602.

(64) The PS-2 reaction center cannot use carotenoids for photoprotection (quenching of chlorophyll triplet states) because its high redox potential would lead to an oxidation of the carotenoids. Because of the shallow trap, however, some of the excitations will escape the reaction center and the subsequently occurring triplet states can be quenched by the carotenoids in the antennae (J. Barber, private communication).